Journal of Network Intelligence
Taiwan Ubiquitous Information
 ISSN 2414-8105 (Online)
Volume **6**, Number **4**, November **2021**

An Improved Spatial Context Based Sparse Unmixing of Hyperspectral Image

Fan Li*

Jiangxi Province Key Laboratory of Water Information
Cooperative Sensing and Intelligent Processing,
Nanchang Institute of Technology, Nanchang 330099, China
lifan@nit.edu.cn

Received August 2021; revised October 2021
*Corresponding author: Fan Li(lifan@nit.edu.cn)

Abstract. *Sparse unmixing aims to find a set of endmembers from a known spectral library that can optimally model mixed pixels taking the fractional abundance as the weight, which is widely applied to hyperspectral image interpretation. It is generally an ill-posed inverse problem and sparse regularization is conducive to obtaining a unique solution. In recent years, spatial information has been regarded as important prior knowledge for unmixing and the exploration of structured information has greatly improved the performance of sparse unmixing. However, most spatial regularization strategies assume that the abundance vectors of neighboring pixels are straightforward smoothness, while ignoring the possible sharp changes between the abundance vectors. To overcome this drawback, we propose an improved spatial context based sparse unmixing algorithm to smooth the estimated abundance map while preserving the edges in the map. Specifically, the bilateral filter is incorporated into the traditional TV regularization to further enhance piecewise smooth transitions in estimated fractional abundances, and the weight based on spatial context information is integrated into the classic ℓ_1 norm regularizer to induce the abundance vectors of neighboring pixels to be correlated. We conduct two sets of simulated data and a set of real data experiments to verify the performance of the proposed algorithm. Experimental results show that our algorithm achieves higher accuracy on abundance estimation than several advanced spatial regularization sparse unmixing algorithms, due to better preservation of spatial texture and edge information.*

Keywords: Hyperspectral image, Sparse unmixing, Spatial weight, Bilateral filter, Total variation(TV).

1. **Introduction.** Hyperspectral imaging technology can collect fine spectral information and rich spatial information simultaneously, which provides high spectral resolution data for practical applications such as mineral exploration, agricultural monitoring, and target detection [1]. However, the spatial resolution of hyperspectral images is insufficient. When the ground object distribution is complex in the scene, there are many mixed pixels present in the image [2]. For better image interpretation, we decompose the mixed pixels into proportional combinations of materials, where each material has pure spectral signature, called endmember, and this fractional proportion is called abundance [3]. With the increase of available spectral libraries, a series of hyperspectral unmixing methods based on sparse regression have been proposed [4]. Sparse unmixing finds the endmembers involved in modeling the image from a priori spectral library instead of a special endmember extraction process, and the abundance estimation becomes the main task of

sparse unmixing [5]. The abundance estimation based on a large spectral library and an observed hyperspectral images is generally an ill-posed inverse problem, which can benefit from sparse regularization in obtaining a unique solution. Some regularization terms, such as ℓ_1 norm, $\ell_p(0 < p < 1)$ norm and $\ell_{2,1}$ mixed norm, serve for the sparsity induction of fractional abundances successively [5–8]. Although sparse-induced unmixing methods have achieved the expected results in abundance estimation, the sparsity measures used in these methods are not enough for the actual sparse degree of fractional abundances, and the correlation between the abundance vectors brought about by the spatial distribution of pixels in the image is ignored.

The weighted ℓ_1 norm minimization strategy is proven to effectively enhance the sparsity of the solution, which outperforms the original ℓ_1 norm [9]. The double reweighted sparse unmixing (DRSU) algorithm designs two weights to promote the row sparsity of the abundance matrix and the sparsity of the fractional abundances with regards to each endmember respectively [10]. The spectral-spatial weighted sparse unmixing (S^2WSU) algorithm modifies the weights in the spatial domain in DRSU, and the new spatial weights are computed from the abundance values of neighboring pixels in each iteration, which enhances the sparsity of the fractional abundances while improving the correlation between the abundance vectors in the neighborhood [11]. The weighted sparse strategy has the immense potential in improving sparse unmixing performance.

In recent years, spatial information has been regarded as important prior knowledge for unmixing and the exploration of structured information has greatly improved the performance of sparse unmixing [12–15]. The sparse unmixing via variable splitting augmented Lagrangian and total variation (SUnSAL-TV) algorithm, as a pioneering work on integrating spatial context information in sparse unmixing, includes the nonisotropic total variation (TV) term to the sparse-induced unmixing model [16]. The TV term promotes neighboring pixels to have similar abundance vectors, which improves the constraints on the ill-posed problem of abundance estimation. Since the TV regularization term makes full use of the spatial homogeneity of the image, it is often included in the sparse unmixing model together with other regularization terms along with other regularization terms. For example, the double reweighted sparse unmixing and total variation (DRSU-TV) algorithm integrates the TV term to a double weighted ℓ_1 norm sparse regression formulation [17]. The superpixel-based reweighted low-rank and total variation (SUSRLR-TV) algorithm combines the TV term with the low-rank constraint on the abundance vectors in the same superpixel block [18]. However, the abovementioned sparse unmixing model including TV spatial regularization may produce oversmooth abundance maps and lead to staircase effects, since the sparsity in the gradient domain is strictly constrained and the sharp edges in the image are not well preserved.

To overcome this drawback, we propose an improved spatial context based sparse unmixing algorithm to smooth the estimated abundance map while preserving the edges in the map. The proposed spatial weighted sparse unmixing with bilateral filter based TV regularization (BTVSWSU) algorithm incorporates the bilateral filter into traditional TV regularization to improve piecewise smooth transitions in estimated fractional abundance maps, and integrates the weight based on spatial context information into the classic ℓ_1 norm regularizer to induce the abundance vectors of neighboring pixels to be correlated. The optimization problem is solved by the alternating direction method of multipliers (ADMM) [19]. We conduct two sets of simulated data and a set of real data experiments to verify the performance of the proposed algorithm. Experimental results show that our algorithm achieves higher accuracy on abundance estimation than several advanced spatial regularization sparse unmixing algorithms, due to better preservation of spatial texture and edge information.

The rest of this paper is organized as follows. Section 2 briefly reviews sparse unmixing and bilateral filtering. Section 3 presents the proposed spatial weighted sparse unmixing with bilateral filter based total variation. The results of simulated and real data experiments are described in section 4. Section 5 draws conclusions from the paper and gives future research prospects.

2. Related Works.

2.1. Sparse unmixing.

Let $\mathbf{Y} \in \mathbb{R}^{L\times n}$ be an observed hyperspectral image composed of n pixels ,with L bands. Let $\mathbf{A} \in \mathbb{R}^{L\times m}$ be an overcomplete spectral library containing m materials. Based on the linear mixture model (LMM), the hyperspectral image can be modeled as:

$$\mathbf{Y} = \mathbf{AX} + \mathbf{N} \tag{1}$$

where $\mathbf{X} \in \mathbb{R}^{m\times n}$ denotes the abundance matrix, and $\mathbf{N} \in \mathbb{R}^{L\times n}$ is noise and model error. Following literature [5], we execute the abundance nonnegative constraint (ANC)(i.e., $\mathbf{X} \geq 0$) but not the abundance sum-to-one constraint (ASC)(i.e., $\mathbf{1}^T\mathbf{x} = 1$).

Since the actual endmembers present in a given scene are much fewer than the materials in the library $\mathbf{A}$, the abundance matrix $\mathbf{X}$ corresponding to $\mathbf{A}$ is sparse. Therefore, the unmixing problem can be converted to a sparse regression problem, the goal of which is to find the optimal subset of entries in the spectral library that can model the image, under the sparse constraint. The constrained optimization problem is formulated as:

$$\min_{\mathbf{X}} \ \frac{1}{2}||\mathbf{Y} - \mathbf{AX}||_F^2 + \lambda||\mathbf{X}||_0 \ \text{s.t.} \quad \mathbf{X} \geq 0 \tag{2}$$

where $||\mathbf{Y} - \mathbf{AX}||_F^2$ denotes the data fidelity item, $||\cdot||_F$ denotes the Frobenius norm, $\|\mathrm{X}\|_0$ denotes the number of zeros in $\mathbf{X}$, and λ is a nonnegative regularization parameter. The problem (2) is an NP (non-deterministic polynomial) problem, which is hard to solve. The ℓ_0 norm can be replaced by the ℓ_1 norm under certain conditions [20, 21]. Then, the following convex optimization problem is obtained:

$$\min_{\mathbf{X}} \ \frac{1}{2}||\mathbf{Y} - \mathbf{AX}||_F^2 + \lambda||\mathbf{X}||_{1,1} \ \text{s.t.} \quad \mathbf{X} \geq 0 \tag{3}$$

where $||\mathbf{X}||_{1,1} = \sum_{j=1}^{n} ||\mathbf{x}_j||_1$ and $\mathbf{x}_j$ denotes the jth column of $\mathbf{X}$. The problem (3) has been solved by the SUnSAL algorithm. Nevertheless, the ℓ_1 norm in problem (3) suggests that each pixel in hyperspectral images is treated as an independent component. In fact, the correlation between the observed spectra of each pixel in the image, which can be mapped to the similarity of abundance vectors, is closely related to the spatial distribution of the pixels. Therefore, spatial information is highly valued in sparse unmixing tasks.

For the piecewise smoothness of the abundance map, the SUnSAL-TV algorithm includes a vector TV term in (2), which exploits spatial context information [16]. The resulting optimization problem is formulated as follows:

$$\min_{\mathbf{X}} \ \frac{1}{2}||\mathbf{Y} - \mathbf{AX}||_F^2 + \lambda||\mathbf{X}||_{1,1} + \lambda_{TV}\mathbf{TV}(\mathbf{X}) \ \text{s.t.} \quad \mathbf{X} \geq 0 \tag{4}$$

where

$$\mathbf{TV}(\mathbf{X}) \equiv \sum_{\{i,j\}\in\varepsilon} ||\mathbf{x}_i - \mathbf{x}_j||_1, \tag{5}$$

denotes the nonisotropic TV in vector form, ε denotes the set of neighbors on the horizontal and vertical directions, and $\lambda_{TV} \geq 0$ is a regularization parameter. The SUnSAL-TV algorithm focuses on a certain aspect of spatial structure characteristics, that is, spatial homogeneity, but does not take into account the sharp changes in fractional abundances at the edges, which leads to the staircase effect.

2.2. **Bilateral filter.** Bilateral filter (BF) is a well-known technique that can smooth the image while preserving the edges, thus it has been rapidly developed in image processing applications [22–24]. The bilateral filter replaces each pixel with the weighted average of pixels close to it in space and in range, where the spatial Gaussian weight depends on the spatial distance between two pixels and the range Gaussian weight is associated with the differences between the values of two pixels [25], defined as:

$$\mathbf{BF}(\mathbf{I})_p = \frac{1}{W_p} \sum_{q \epsilon S} G_{\sigma_s}(\|p-q\|) G_{\sigma_r}(|I_p - I_q|) I_q \tag{6}$$

where p denotes the center pixel, q denotes any neighboring pixel of p in the spacial domain s, I denotes the input image, I_p and I_q denote the value of p and q, respectively, $\|p-q\|$ calculates the Euclidean distance between p and q, W_p denotes the normalization factor, calculated as:

$$W_p = \sum_{q \epsilon S} G_{\sigma_s}(\|p-q\|) G_{\sigma_r}(|I_p - I_q|) \tag{7}$$

where

$$G_\sigma(x) = \frac{1}{2\pi\sigma^2} \exp(-\frac{x^2}{2\sigma^2}), \tag{8}$$

denotes the 2D Gaussian kernel and σ is a parameter defining the neighborhood size. Specifically, G_{σ_s} is the spatial Gaussian weight that penalizes distant pixels in the spatial domain s, the farther the distance, the smaller the weight, and G_{σ_r} is the range Gaussian weight that penalizes pixels with significant differences, the greater the difference, the smaller the weight. As a nonlinear technique, bilateral filter multiplies the two weights, so only the nearby similar pixels affect the result, and the result further impact on the central pixel. In other words, if either of the two weights is close to zero, smoothing will not occur. The pixels at the edges are close in space, but obviously have different values, thus they are well preserved due to the rang Gaussian weight.

To sum up, the bilateral filter smoothes the image by weighted average of the pixels in a local area, but limited by the combination of spatial filter and range filter, the edge pixels in the image will not be smoothed.

3. **The Proposed BTVSWSU Algorithm.** Inspired by [11] and [26], we propose an improved spatial context based sparse unmixing model to alleviate the oversmooth phenomenon and staircase effect caused by TV regularization that imposes too strict constraints on spatial context information. The proposed method introduces the spatial weights into the sparse regularization term and the bilateral filter into the TV spatial regularization term, called spatial weighted sparse unmixing with bilateral filter based total variation regularization (BTVSWSU). The model is formulated as follows:

$$\min_{\mathbf{X}} \quad \frac{1}{2}||\mathbf{Y} - \mathbf{A}\mathbf{X}||_F^2 + \lambda \|\mathbf{W}_{spa} \odot \mathbf{X}\|_{1,1} + \lambda_{bf} \mathbf{TV}(\mathbf{BF}(\mathbf{X})) \text{ s.t.} \quad \mathbf{X} \geq 0 \tag{9}$$

where $\odot$ is an operator that denotes the Hadamard product, i.e., element-wise product of two matrixes. The spatial weight matrix $\mathbf{W}_{spa} \in \mathbb{R}^{m \times n}$ is computed according to the abundance vectors of neighboring pixels [11], defined as:

$$w_{spa,ij} = \frac{1}{f_{h \in \mathcal{N}(j)}(x_{ih}) + \varepsilon} \tag{10}$$

where $w_{spa,ij}$ denotes the element of the ith row and jth column in $\mathbf{W}_{spa}$, $\mathcal{N}(j)$ denotes the neighborhood set of the pixel corresponding to the jth column vector of the abundance matrix $\mathbf{X}$, $f(\cdot)$ is a function for exploring spatial context information, which can be constructed in various ways, such as linear or nonlinear and local and nonlocal [27–32], $\varepsilon >$

0 is a small constant to avoid singularities. In our work, function $f(\cdot)$ row-wise calculates the weighted average of the fractional abundances corresponding to the neighboring pixels, and x_{ih} denotes the ith value(band) in the abundance vector corresponding to any pixel in $\mathcal{N}(j)$, which is defined as follows:

$$f(x_{ij}) = \frac{\sum_{h\in\mathcal{N}(j)} d(p_j, p_h)x_{ih}}{\sum_{h\in\mathcal{N}(j)} d(p_j, p_h)} \tag{11}$$

where p_j denotes the center pixel corresponding to the fractional abundance x_{ij}, p_h denotes any pixel in the $\mathcal{N}(j)$, x_{ih} is the ith value in the abundance vector of pixel p_h, and $d(p_j, p_h)$ denotes the Euclidean distance between pixel p_j and pixel p_h, The spatial weight matrix $\mathbf{W}_{spa}$ is updated iteratively. When the fractional abundances of neighboring pixels are large, the spatial weight is small. Therefore, the abundance matrix will be guided to be sparse by the weight in the iterations. Note that it will not eliminate small differences between abundance vectors of neighboring pixels, thereby improving the oversmooth phenomenon of the estimated abundance maps.

In addition, the integration of the bilateral filter into the TV term can effectively alleviate the staircase effect [26]. In the model (9), TV regularization is implemented on the result of bilateral filtering the abundance matrix $\mathbf{X}$, but not directly on $\mathbf{X}$. $\lambda_{bf} \geq 0$ is the regularization parameter for the bilateral filter based TV.

The proposed BTVSWSU model simultaneously enforced the spatial weighted sparse constraint and the bilateral filter based TV regularizer in the process of abundance estimation. The above multiple constraint strategy is designed from the structural characteristics of the spatial distribution of pixels, which effectively utilizes spatial context information and can mitigate the negative effects of oversmooth phenomenon and staircase effect caused by the TV regularization.

We solve the optimization model (9) in the ADMM framework. In order to accelerate the convergence of the algorithm, we adopt the inner and outer loops solution, the space weight matrix $\mathbf{W}_{spa}$ is updated in the outer loop, and the fractional abundances are solved by ADMM in the inner loop.

Let $\mathbf{H}$ be the linear operators calculating the differences between the horizontal and vertical components of the abundance matrix $\mathbf{X}$. The original problem will be split into several subproblems by introducing auxiliary matrix variables $\mathbf{U}$, $\mathbf{V}_1$, $\mathbf{V}_2$, $\mathbf{V}_3$, $\mathbf{V}_4$, $\mathbf{V}_5$, $\mathbf{V}_6$. Therefore, the objective function is rewritten as follows:

$$\begin{aligned} \min_{\mathbf{U},\mathbf{V}_1,\mathbf{V}_2,\mathbf{V}_3,\mathbf{V}_4,\mathbf{V}_5,\mathbf{V}_6} & \frac{1}{2}\|\mathbf{Y}-\mathbf{V}_1\|_F^2 + \lambda\|\mathbf{W}_{spa}\odot\mathbf{V}_2\|_{1,1} + \lambda_{bf}\|\mathbf{V}_5\|_{1,1} + \iota_{R+}(\mathbf{V}_6) \\ \text{s.t.} \quad & \mathbf{V}_1 = \mathbf{A}\mathbf{U}, \mathbf{V}_2 = \mathbf{U}, \mathbf{V}_3 = \mathbf{U}, \mathbf{V}_4 = \mathbf{B}\mathbf{F}(\mathbf{V}_3), \mathbf{V}_5 = \mathbf{H}\mathbf{V}_4, \mathbf{V}_6 = \mathbf{U} \end{aligned} \tag{12}$$

where $\mathbf{U} = \mathbf{X}$, $\iota_{R+}(\mathbf{X}) = \sum_{i=1}^{n} \iota_{R+}(\mathbf{x}_i)$ is an indicator function that $\iota_{R+}(\mathbf{x}_i)$ is zero if $\mathbf{x}_i \geq 0$, and $+\infty$ otherwise. Let $\mathbf{K}\mathbf{V}_3$ linearly replace $\mathbf{B}\mathbf{F}(\mathbf{V}_3)$ and define

$$\mathbf{G}=\begin{bmatrix}\mathbf{A}\\ \mathbf{I}\\ \mathbf{I}\\ \mathbf{0}\\ \mathbf{0}\\ \mathbf{I}\end{bmatrix}, \quad \mathbf{B}=\begin{bmatrix}\text{-}\mathbf{I} & 0 & 0 & 0 & 0 & 0\\ 0 & \text{-}\mathbf{I} & 0 & 0 & 0 & 0\\ 0 & 0 & \text{-}\mathbf{I} & 0 & 0 & 0\\ 0 & 0 & \mathbf{K} & \text{-}\mathbf{I} & 0 & 0\\ 0 & 0 & 0 & \mathbf{H} & \text{-}\mathbf{I} & 0\\ 0 & 0 & 0 & 0 & 0 & \text{-}\mathbf{I},\end{bmatrix}, \quad \mathbf{V}=\begin{bmatrix}\mathbf{V}_1\\ \mathbf{V}_2\\ \mathbf{V}_3\\ \mathbf{V}_4\\ \mathbf{V}_5\\ \mathbf{V}_6\end{bmatrix},$$

$$g(\mathbf{V}) = \frac{1}{2}\|\mathbf{Y}-\mathbf{V}_1\|_F^2 + \lambda\|\mathbf{W}_{spa}\odot\mathbf{V}_2\|_{1,1} + \lambda_{bf}\|\mathbf{V}_5\|_{1,1} + \iota_{R+}(\mathbf{V}_6) \tag{13}$$

The objective function (12) can be represented in a compact form:

$$\min_{\mathbf{U},\mathbf{V}} \ g(\mathbf{V}) \ \text{ s.t. } \mathbf{GU}+\mathbf{BV}=\mathbf{0} \tag{14}$$

And the augmented Lagrangian for (14) is:

$$\mathcal{L}(\mathbf{U},\mathbf{V},\mathbf{D}) = g(\mathbf{V}) + \frac{\mu}{2}\|\mathbf{GU}+\mathbf{BV}-\mathbf{D}\|_F^2 \tag{15}$$

where $\mu > 0$ is the penalty parameter, $\mathbf{D} = (\mathbf{D}_1, \mathbf{D}_2, \mathbf{D}_3, \mathbf{D}_4, \mathbf{D}_5, \mathbf{D}_6)$ is the Lagrange multipliers. In each iteration, the ADMM minimizes $\mathcal{L}(\mathbf{U},\mathbf{V},\mathbf{D})$ with respect to $\mathbf{U}$ and $\mathbf{V}$, and updates $\mathbf{D}$, as follows:

$$\begin{cases} \mathbf{U}^{(k+1)} = \arg\min_{\mathbf{U}} \mathcal{L}(\mathbf{U}, \mathbf{V}^{(k)}, \mathbf{D}^{(k)}) \\ \mathbf{V}^{(k+1)} = \arg\min_{\mathbf{V}} \mathcal{L}(\mathbf{U}^{(k+1)}, \mathbf{V}, \mathbf{D}^{(k)}) \\ \mathbf{D}^{(k+1)} = \mathbf{D}^{(k)} - \mathbf{GU}^{(k+1)} - \mathbf{BV}^{(k+1)} \end{cases} \tag{16}$$

By solving the subproblems in (16), we obtain the proposed BTVSWSU algorithm, as shown in Algorithm 1, where $\text{soft}(\cdot,\tau)$ denotes the soft-threshold function $y \mapsto \text{sign}(y)\max\{|y|-\tau, 0\}$.

Algorithm 1 Pseudocode of the BTVSWSU algorithm

Initialization:
set $k, t = 0$, choose $\mu, \lambda, \lambda_{bf}, \varepsilon > 0, \mathbf{U}^{(0)}, \mathbf{V}_i^{(0)}, \mathbf{D}_i^{(0)}$, for $i = 1, \ldots, 6$

Repeat:
Update $\mathbf{W}_{spa}^{(t)}$ using (10) and (11)
Repeat:
$\mathbf{U}^{(k+1)} \leftarrow (\mathbf{A^T A} + 3\mathbf{I})^{-1}(\mathbf{A^T}(\mathbf{V}_1^{(k)} + \mathbf{D}_1^{(k)}) + \mathbf{V}_2^{(k)} + \mathbf{D}_2^{(k)} + \mathbf{V}_3^{(k)} + \mathbf{D}_3^{(k)} + \mathbf{V}_6^{(k)} + \mathbf{D}_6^{(k)})$
$\mathbf{V}_1^{(k+1)} \leftarrow \frac{1}{1+\mu}[\mathbf{Y} + \mu(\mathbf{AU}^{(k+1)} - \mathbf{D}_1^{(k)})]$
$\mathbf{V}_2^{(k+1)} \leftarrow \text{soft}(\mathbf{U}^{(k+1)} - \mathbf{D}_2^{(k)}, \frac{\lambda}{\mu}\mathbf{W}_{spa}^{(t)})$
$\mathbf{V}_3^{(k+1)} \leftarrow \frac{1}{2}(\mathbf{V}_4^{(k)} + \mathbf{D}_4^{(k)}) + \frac{1}{2}(\mathbf{U}^{(k+1)} - \mathbf{D}_3^{(k)})$
$\mathbf{V}_4^{(k+1)} \leftarrow (\mathbf{I} + \mathbf{H}^T\mathbf{H})^{-1}(\mathbf{BF}(\mathbf{V}_3^{(k+1)}) - \mathbf{D}_4^{(k)} + \mathbf{H}^T\mathbf{V}_5^{(k)} + \mathbf{H}^T\mathbf{D}_5^{(k)})$
$\mathbf{V}_5^{(k+1)} \leftarrow \text{soft}(\mathbf{HV}_4^{(k+1)} - \mathbf{D}_5^{(k)}, \frac{\lambda_{bf}}{\mu})$
$\mathbf{V}_6^{(k+1)} \leftarrow \max(\mathbf{U}^{(k+1)} - \mathbf{D}_6^{(k)}, 0)$
Update Lagrange multipliers:
$\mathbf{D}_1^{(k+1)} \leftarrow \mathbf{D}_1^{(k)} - \mathbf{AU}^{(k+1)} + \mathbf{V}_1^{(k+1)}$
$\mathbf{D}_2^{(k+1)} \leftarrow \mathbf{D}_2^{(k)} - \mathbf{U}^{(k+1)} + \mathbf{V}_2^{(k+1)}$
$\mathbf{D}_3^{(k+1)} \leftarrow \mathbf{D}_3^{(k)} - \mathbf{U}^{(k+1)} + \mathbf{V}_3^{(k+1)}$
$\mathbf{D}_4^{(k+1)} \leftarrow \mathbf{D}_4^{(k)} - \mathbf{BF}(\mathbf{V}_3^{(k+1)}) + \mathbf{V}_4^{(k+1)}$
$\mathbf{D}_5^{(k+1)} \leftarrow \mathbf{D}_5^{(k)} - \mathbf{HV}_4^{(k+1)} + \mathbf{V}_5^{(k+1)}$
$\mathbf{D}_6^{(k+1)} \leftarrow \mathbf{D}_6^{(k)} - \mathbf{U}^{(k+1)} + \mathbf{V}_6^{(k+1)}$
Update: $k \leftarrow k+1$
$\mathbf{U}^{(t+1)} \leftarrow \mathbf{U}^{(k)}$
$\mathbf{D}_2^{(t+1)} \leftarrow \mathbf{D}_2^{(k)}$
Update: $t \leftarrow t+1$
until some stopping criterion is satisfied.

Note that the proposed BTVSWSU algorithm stops when the maximum number of iterations is reached or the residual $||\mathbf{GU}^{(t)} + \mathbf{BV}^{(t)}||_F$ meets the *threshold* (Usually a

small positive value, such as 1e−5). Moreover, the inner loop and out loop are empirically set to 5 and 60 iterations, respectively, which guarantees the convergence of the proposed algorithm.

4. **Experiment and Analysis.**

4.1. **Experiment on simulated hyperspectral data.** In this section, we perform the proposed BTVSWSU algorithm on two simulated hyperspectral data sets to illustrate its unmixing performance. Four advanced sparse unmixing algorithms, namely SUnSAL [5], CLSUnSAL [7], SUnSAL-TV [16] and SUnSAL-BF-TV [26], are performed on the same simulated data. There are two spectral libraries used in the experiments, which are selected from the USGS splib06 library[1]. The spectral library $\mathbf{A_1} \in \mathbb{R}^{224\times240}$ is comprised of 240 spectral signatures with 224 bands uniformly covering the range from $0.4\mu m$ to $2.5\mu m$. The spectral library $\mathbf{A_2} \in \mathbb{R}^{221\times222}$ contains $m = 222$ spectral signatures with 221 bands. Two sets of simulated data are generated by the endmembers selected from the above spectral library and the abundance maps satisfying ANC and ASC.

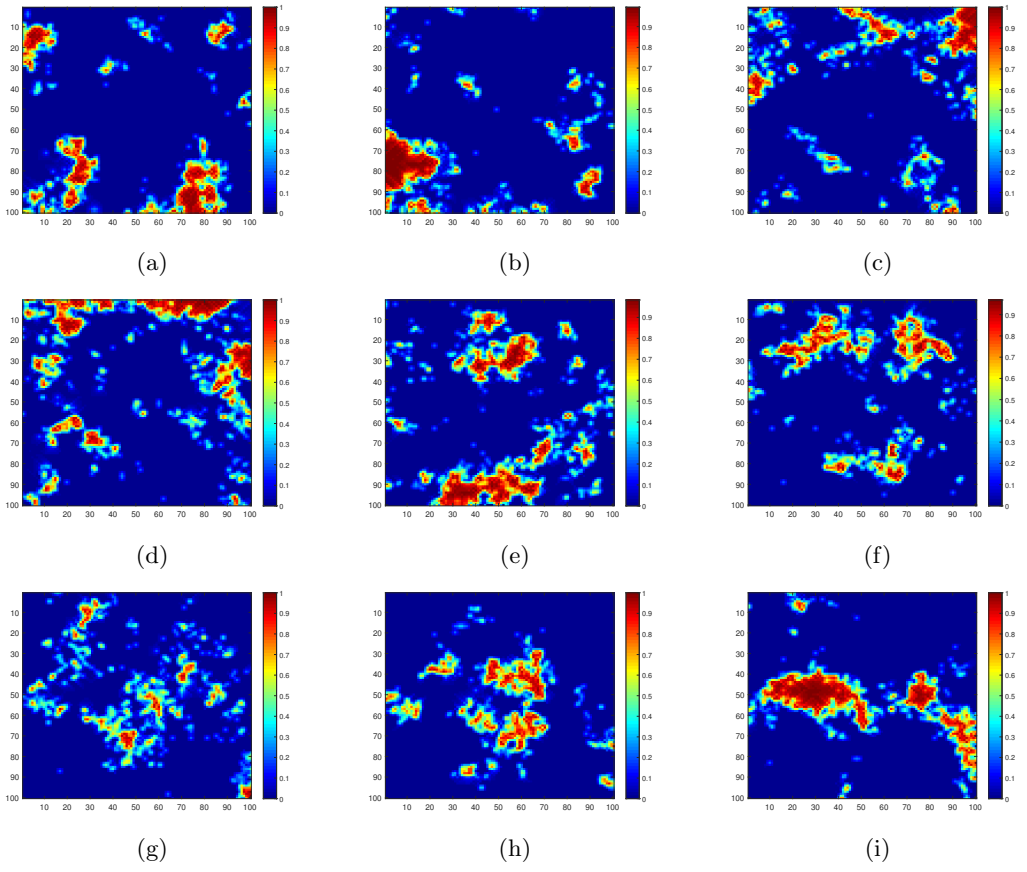

FIGURE 1. True abundance map of nine endmembers in DC1. (a)endmember1, (b)endmember2, (c)endmember3, (d)endmember4, (e)endmember5, (f)endmember6, (g)endmember7, (h)endmember8, (i)endmember9.

- Simulated Data Cube 1 (DC1): It is generated by nine endmember from the library $\mathbf{A_1}$ and contains 100×100 pixels. The abundance maps used in this data set are piecewise smooth, as shown in Figure 1. The data is subsequently contaminated by

[1]http://speclab.cr.usgs.gov/spectral.lib06.

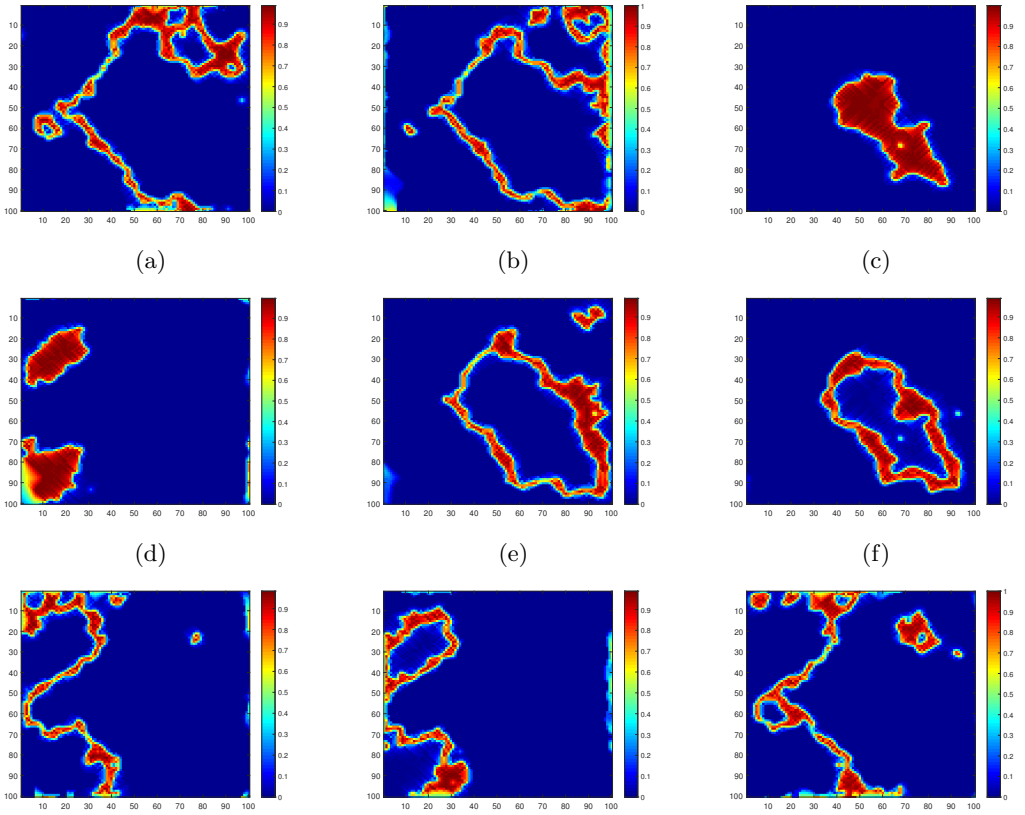

FIGURE 2. True abundance map of nine endmembers in DC2. (a)endmember1, (b)endmember2, (c)endmember3, (d)endmember4, (e)endmember5, (f)endmember6, (g)endmember7, (h)endmember8, (i)endmember9.

i.i.d. Gaussian noise with four levels of the signal-to-noise (SNR) ratio:20, 30, 40 and 50dB.

- Simulated Data Cube 2 (DC2): It is generated by nine endmember from the library $\mathbf{A_2}$ and contains 100×100 pixels. The abundance maps used in this data are created by fractals that imitate the spatial patterns of nature [33,34], as shown in Figure 2. In the same vein, the data is subsequently contaminated by i.i.d. Gaussian noise with SNR=20, 30, 40 and 50dB.

Two performance discriminators are adopted to quantitatively evaluate the quality of the results obtained by different algorithms in simulated data experiment. The signal to reconstruction error (SRE(dB)) is defined as:

$$\text{SRE(dB)} = 10 \cdot \log_{10}(E(||\mathbf{x}||_2^2)/E(||\mathbf{x} - \widehat{\mathbf{x}}||_2^2)), \tag{17}$$

where $\mathbf{x}$ denotes the actural abundance, $\widehat{\mathbf{x}}$ denoted the estimated abundance and $E(\cdot)$ denotes the expectation function. Furthermore, the probability of success p_s, defined as $p_s \equiv P(\|\widehat{\mathbf{x}}-\mathbf{x}\|^2/\|\mathbf{x}\|^2 \leq threshold)$, is another indicator for quantitative evaluation. The results can be considered as successful, when $\|\widehat{\mathbf{x}}-\mathbf{x}\|^2/\|\mathbf{x}\|^2 \leq 3.16$ (5dB) [5]. The higher the SRE(dB) or p_s, the better the unmixing performance.

Two sets of simulated data are unmixed by the proposed BTVSWSU algorithm and the comparison algorithms. SRE(dB) and p_s values of the results are shown in Tables 1 and 2, respectively. The optimal parameters are list in the parentheses. It can be seen

TABLE 1. SRE(dB) and p_s values of the results obtained by different algorithms on DC1 (the optimal parameters for the reported results are listed in parentheses).

Algorithm	**SNR=20dB**		**SNR=30dB**		**SNR=40dB**		**SNR=50dB**	
	SRE(dB)	p_s	SRE(dB)	p_s	SRE(dB)	p_s	SRE(dB)	p_s
SUnSAL	4.1978	0.5561	8.4831	0.7979	15.1817	0.9907	23.0236	1
	(λ = 2e-1)		(λ = 2e-2)		(λ = 5e-3)		(λ = 1e-3)	
CLSUnSAL	3.4040	0.4692	6.5520	0.7265	11.4404	0.9693	20.4946	1
	(λ = 2.3)		(λ = 4e-1)		(λ = 2e-2)		(λ = 8e-3)	
SUnSAL-TV	6.3542	0.6625	11.4698	0.9475	17.7609	0.9998	26.0960	1
	(λ = 2e-2; λ_{TV} = 2e-2)		(λ = 1e-2; λ_{TV} = 4e-3)		(λ = 5e-3; λ_{TV} = 1e-3)		(λ = 2e-3; λ_{TV} = 2e-4)	
SUnSAL-BF-TV	7.3712	0.7505	14.6634	0.9662	19.8747	0.9927	28.5930	1
	(λ = 2e-3; λ_{bf} = 2e-2)		(λ = 5e-4; λ_{bf} = 4e-3)		(λ = 2e-4; λ_{bf} = 2e-3)		(λ = 6e-5; λ_{bf} = 6e-4)	
BTVSWSU	8.7233	0.8357	17.1927	0.9865	27.0796	1	38.3879	1
	(λ = 2e-3; λ_{bf} = 9e-3)		(λ = 4e-4; λ_{bf} = 2e-3)		(λ = 9e-5; λ_{bf} = 1e-4)		(λ = 2e-5; λ_{bf} = 8e-6)	

TABLE 2. SRE(dB) and p_s values of the results obtained by different algorithms on DC2 (the optimal parameters for the reported results are listed in parentheses).

Algorithm	**SNR=20dB**		**SNR=30dB**		**SNR=40dB**		**SNR=50dB**	
	SRE(dB)	p_s	SRE(dB)	p_s	SRE(dB)	p_s	SRE(dB)	p_s
SUnSAL	4.4049	0.5956	10.1453	0.9087	17.7791	0.9966	26.1174	1
	(λ = 1e-1)		(λ = 1e-2)		(λ = 3e-3)		(λ = 9e-4)	
CLSUnSAL	2.8263	0.3635	7.1121	0.7078	11.4179	0.8963	13.4230	0.9400
	(λ = 8e-1)		(λ = 3e-1)		(λ = 8e-3)		(λ = 6e-3)	
SUnSAL-TV	7.3829	0.7912	14.8342	0.9974	23.1805	0.9999	30.7843	1
	(λ = 1e-2; λ_{TV} = 1e-2)		(λ = 3e-3; λ_{TV} = 4e-3)		(λ = 1e-3; λ_{TV} = 1e-3)		(λ = 9e-4; λ_{TV} = 3e-4)	
SUnSAL-BF-TV	16.0312	0.9945	23.0448	0.9997	31.0235	1	39.9956	1
	(λ = 6e-3; λ_{bf} = 3e-2)		(λ = 5e-4; λ_{bf} = 5e-3)		(λ = 2e-4; λ_{bf} = 1e-3)		(λ = 5e-5; λ_{bf} = 2e-4)	
BTVSWSU	18.2817	0.9950	25.9149	0.9998	34.8198	1	42.7504	1
	(λ = 3e-3; λ_{bf} = 2e-2)		(λ = 4e-4; λ_{bf} = 2e-3)		(λ = 1e-4; λ_{bf} = 3e-4)		(λ = 4e-5; λ_{bf} = 5e-6)	

from Tables 1 and 2 that the proposed BTVSWSU algorithm has the highest SRE(dB) in all cases, and retains higher p_s in the case of high noise. Compared with SUnSAL-TV algorithm, the performance of SUnSAL-BF-TV algorithm is significantly improved due to the involvement of bilateral filter. The BTVSWSU algorithm shows greater advantages than SUnSAL-BF-TV, which verifies the effect of spatial weights.

To further illustrate the effectiveness of the proposed BTVSWSU algorithm, we take the results obtained by performing each algorithm on DC1 with SNR=30dB as an example for visual exhibition and comparison. Figure 3 shows the actual abundance and the resulting estimated abundances, and only 100 randomly selected pixels are displayed for better visual effects. The lines indicate the endmembers which are selected from the spectral library to participate in modeling the hyperspectral image. It can be seen from Figure 3 that the number of endmembers found by the SUnSAL-BF-TV and BTVSWSU algorithms is consistent with the number of actual endmembers, while the abundance map obtained

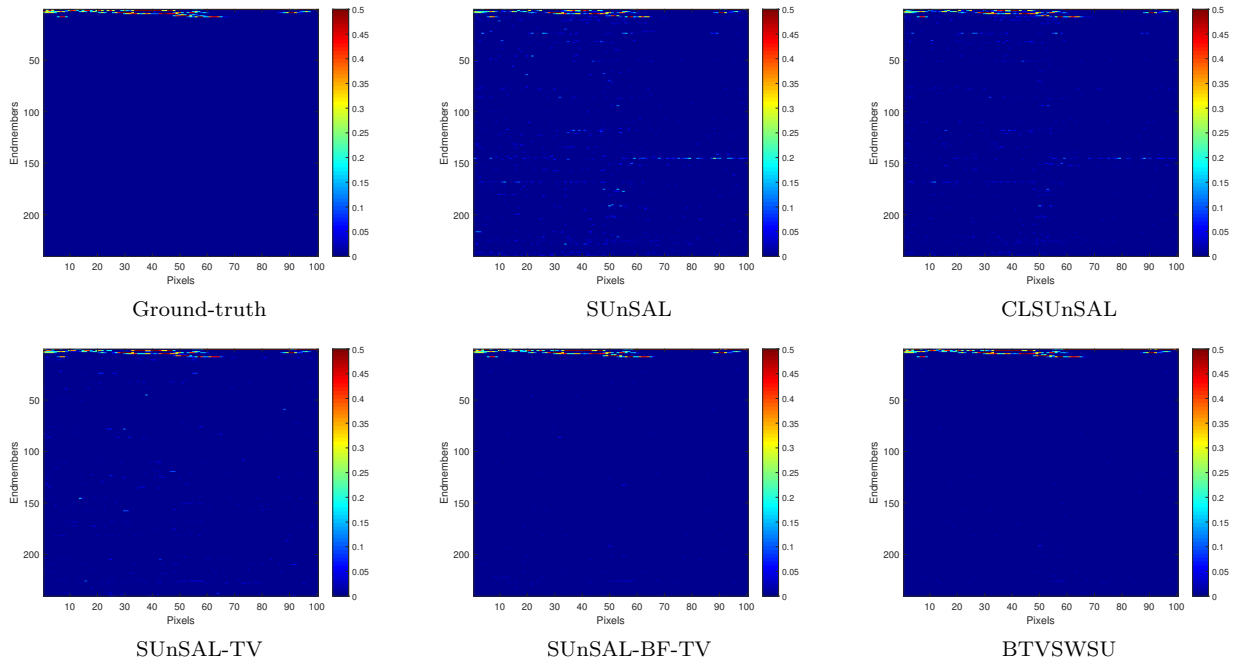

FIGURE 3. The true abundance and estimated abundances obtained by performing BTVSWSU and comparison algorithms on DC1 with SNR=30dB.

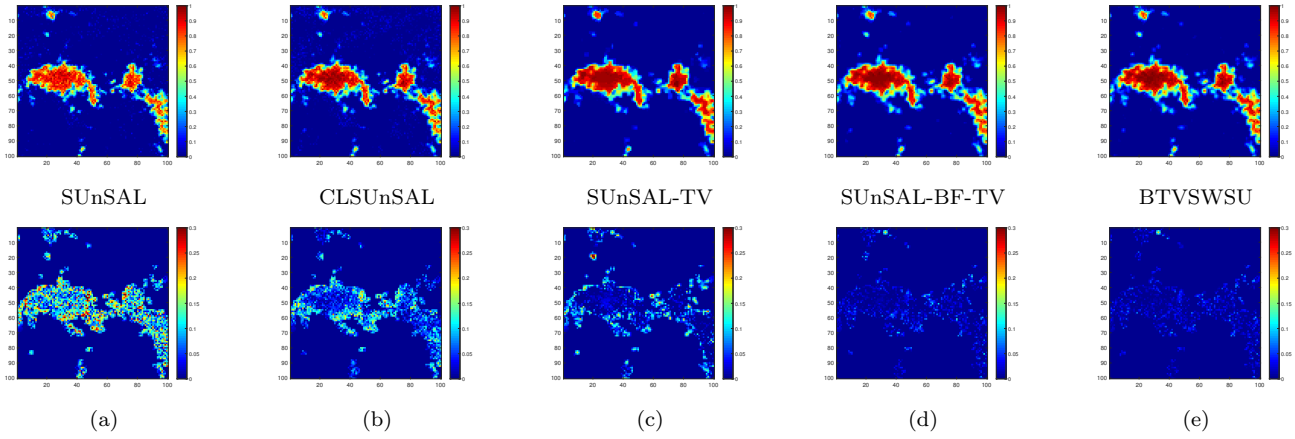

FIGURE 4. Abundance maps of endmember1 obtained by performing BTVSWSU and comparison algorithms on DC1 with SNR=30dB. Differences between the actual abundance and estimated abundances obtained by performing each algorithm on DC1 with SNR=30dB. (a) Differences produced by SUnSAL, (b)Differences produced by CLSUnSAL, (c)Differences produced by SUnSAL-TV, (d)Differences produced by SUnSAL-BF-TV, (e)Differences produced by BTVSWSU.

by the BTVSWSU algorithm is cleaner in the original zeros region with less noise. It can be inferred that the combination of spatial weighted sparse regularization and bilateral filter based TV regularization improves the ability to identify endmembers.

In order to confirm that the proposed BTVSWSU algorithm is effective in overcoming the oversmooth and staircase effect, we show the abundance maps of the first endmembers in DC1 and DC2 obtained by different algorithms when SNR=30dB. The abundance maps

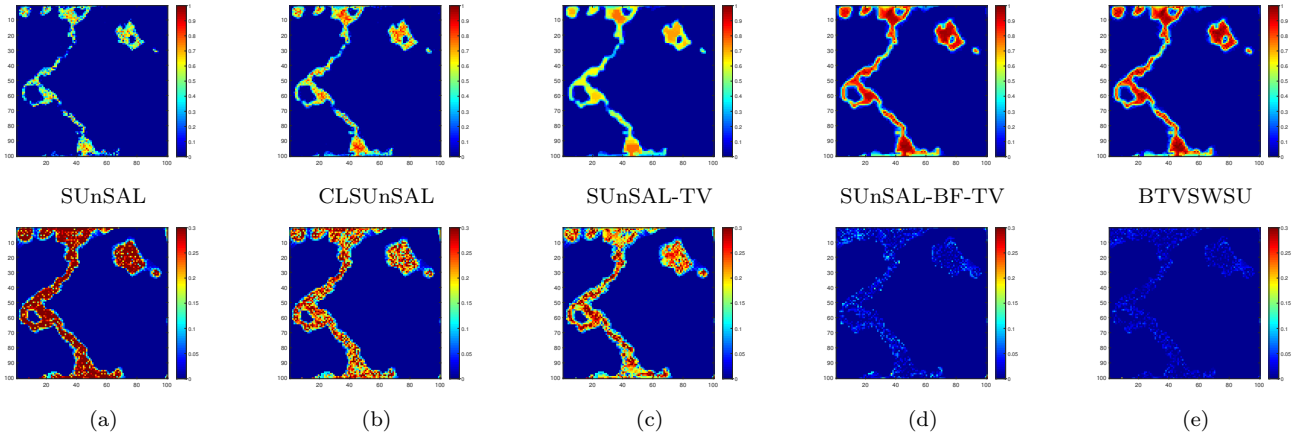

FIGURE 5. Abundance maps of endmember1 obtained by performing BTVSWSU and comparison algorithms on DC2 with SNR=30dB. Differences between the actual abundance and estimated abundances obtained by performing each algorithm on DC2 with SNR=30dB. (a) Differences produced by SUnSAL, (b)Differences produced by CLSUnSAL, (c)Differences produced by SUnSAL-TV, (d)Differences produced by SUnSAL-BF-TV, (e)Differences produced by BTVSWSU.

of other endmembers have similar characteristics, so they are not shown. For visually intuitive comparison, Figures 4 and 5 show the estimated abundance maps of endmember1 from DC1 and DC2 and the difference maps between the actual abundance and the results. It can be clearly seen from the difference maps that the results obtained by our algorithm are closest to the actual abundance maps and the results obtained by SUnSAL and CLSUnSAL are less accurate. In particular, the staircase effect at the edges of the abundance maps obtained by SUnSAL-BF-TV and BTVSWSU algorithms is obviously mitigated compared with the SUnSAL-TV algorithm. The BTVSWSU algorithm solves the issue of oversmooth better than the SUnSAL-BF-TV algorithm, the resulting abundance maps are more accurate in detail. The proposed BTVSWSU algorithm makes full use of spatial context information in hyperspectral images, and improves the unmixing performance significantly.

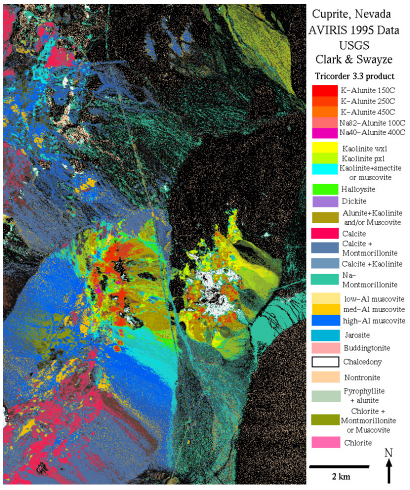

FIGURE 6. USGS map showing the location of different minerals in the Cuprite mining district in Nevada.

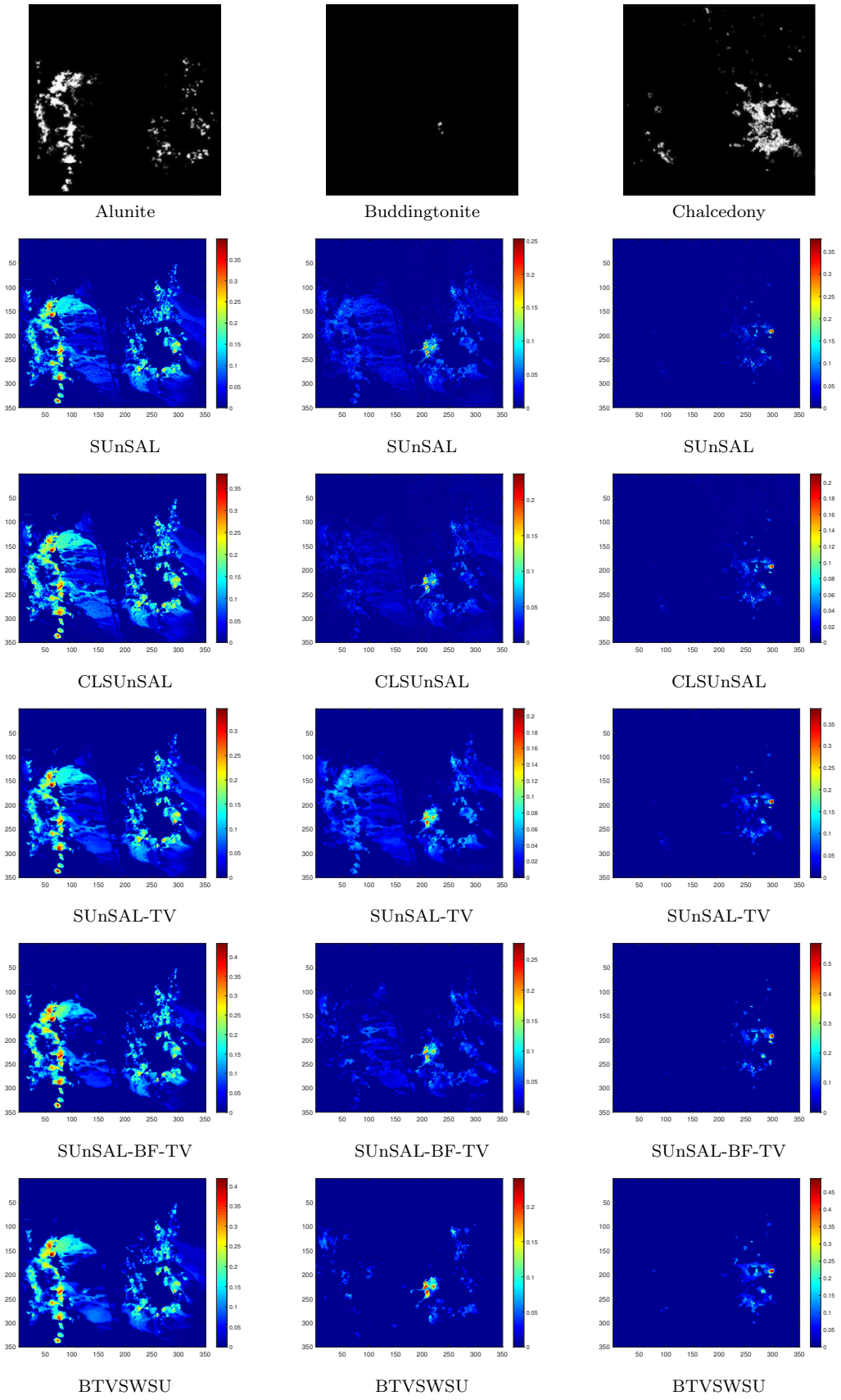

FIGURE 7. Fractional abundances obtained by the BTVSWSU and comparison algorithms on the subset of Cuprite scene.

4.2. **Experiment on real hyperspectral data.** The famous Airborne Visible Infrared Imaging Spectrometer (AVIRIS) Cuprite data set[2], as a common benchmark for the validation of hyperspectral unmixing algorithms, is used in the real data experiment to test the performance of the proposed BTVSWSU algorithm. The portion of the Cuprite data, i.e., the subset of the scene with 350×350 pixels, is used in our experiment. The real data has 224 spectral bands covering the wavelength range from 0.4 μm to 2.5 μm. The bands 1-2, 105-115, 150-170 and 223-224 are removed from the data due to the water absorption and low SNR. The spectral library $\mathbf{A}_1$ used in the simulated experiment is also used for the real data experiment after removing corresponding bands. That is, the library $\mathbf{A}_1 \in \mathbb{R}^{188\times240}$ is used to unmix the Cuprite data. The classification map of the minerals located in Cuprite mining district [3] in Nevada is produced by USGS using Tricorder 3.3 software [4] [35], as shown in Figure 6. The USGS map provides a good reference for the qualitative assessment of the abundance maps obtained by different unmixing algorithms.

Figure 7 shows the abundance maps of three typical minerals (Alunite, Buddingtonite and Chalcedony) obtained by the BTVSWSU and comparison algorithms. The regularization parameters for SUnSAL and CLSUnSAL algorithms were empirically set to $\lambda = 2e\text{-}3$, $\lambda = 2e\text{-}2$, respectively, while the parameters for SUnSAL-TV, SUnSAL-BF-TV and BTVSWSU algorithms were set to $(\lambda = 2e\text{-}3, \lambda_{TV} = 2e\text{-}3)$, $(\lambda = 5e\text{-}4, \lambda_{bf} = 4e\text{-}3)$ and $(\lambda = 4e\text{-}4, \lambda_{bf} = 2e\text{-}3)$, respectively. In addition, we set $\sigma_s = 18$ and $\sigma_r = 0.005$ for the bilateral filter the same as simulated experiments. It can be seen from Figure 7 that all algorithms can interpret the Cuprite data well and obtain reasonable results, where the locations with high fractional abundances indicate the existence of the typical minerals. Nevertheless, some abundance maps (e.g., Buddingtonite) estimated by SUnSAL, CLSUnSAL and SUnSAL-TV is vague due to the noise interference. The results obtained by SUnSAL-TV show that the edge area in the map is oversmooth. Compared to SUnSAL-BF-TV, the fractional abundances estimated by the BTVSWSU algorithm are generally higher or comparable in the regions which are classified as respective minerals. From a qualitatively viewpoint, the improved spatial context information based sparse unmixing algorithm offers great potential on accurate abundance estimation, which effectively overcomes the inherent shortcomings of the traditional spatial regularization sparse unmixing, such as oversmooth and staircase effect.

5. **Conclusions and Future Work.** In this paper, an improved spatial context information based sparse unmixing algorithm is proposed, which introduces spatial weighs into the sparse regularizer and integrates the bilateral filter into the TV spatial regularization term. The spatial weight is constructed based on the abundance vectors of neighboring pixels, which guides abundance matrix to be sparse in the iterations and retains small differences in fractional abundances. The bilateral filter acts on the abundance matrix before performing TV regularization, which smoothes the abundance map while preserving the edges in the map. The proposed BTVSWSU algorithm exploits the spatial structural information by multiple constraints, which effectively alleviates the oversmooth phenomenon and staircase effect. Experimental results show that the proposed BTVSWSU algorithm consistently achieves better performance than several state-of-the-art algorithms in unmixing both simulated and real hyperspectral data. In the future, we will study hyperspectral unmixing formed as the third-order tensor, and develop the bilateral filter for 3D data.

[2]http://aviris.jpl.nasa.gov/html/aviris.freedata.html.
[3]http://speclab.cr.usgs.gov/cuprite95.tgif.2.2um_map.gif.
[4]http://speclab.cr.usgs.gov/PAPER/tetracorder.

Acknowledgment. This work was supported in part by National Natural Science Foundation of China under Grant 61865012, in part by Basic Science and Technology Research Project of National Key Laboratory of Science and Technology on Automatic Target Recognition under Grant WDZC20205500204, in part by Jiangxi Provincial Key Research and Development Program under Grant 20202BBGL73081, Grant 20181ACG70022, in part by the Science and Technology Project of Jiangxi Provincial Department of Education under Grants GJJ170992, GJJ190956.

REFERENCES

[1] J. M. Bioucas-Dias, A. Plaza, G. Camps-Valls, P. Scheunders, N. Nasrabadi and J. Chanussot, Hyperspectral Remote Sensing Data Analysis and Future Challenges, *IEEE Geoscience and Remote Sensing Magazine*, vol.1, no.2, pp.6-36, 2013.

[2] A. Plaza, Q. Du, J. M. Bioucas-Dias, X. Jia and F. A. Kruse, Foreword to the Special Issue on Spectral Unmixing of Remotely Sensed Data, *IEEE Transactions on Geoscience and Remote Sensing*, vol.49, no.11, pp.4103-4110, 2011.

[3] N. Keshava and J. Mustard, Spectral unmixing, *IEEE Signal Processing Magazine*, vol.19, no.1, pp.44-57, 2002.

[4] J. Bioucas-Dias, A. Plaza, N. Dobigeon, M. Parente, Q. Du, P. Gader and J. Chanussot, Hyperspectral Unmixing Overview: Geometrical, Statistical, and Sparse Regression-Based Approaches, *IEEE Journal of Selected Topics in Applied Earth Observations and Remote Sensing*, vol.5, no.2, pp.354-379, 2012.

[5] M. D. Iordache, J. Bioucas-Dias and A. Plaza, Sparse Unmixing of Hyperspectral Data, *IEEE Transactions on Geoscience and Remote Sensing*, vol.49, no.6, pp.2014-2039, 2011.

[6] F. Chen and Y. Zhang, Sparse Hyperspectral Unmixing Based on Constrained $l_p - l_2$ Optimization, *IEEE Geoscience and Remote Sensing Letters*, vol.10, no.5, pp. 1142-1146, 2013.

[7] M. D. Iordache, J. Bioucas-Dias and A. Plaza, Collaborative Sparse Regression for Hyperspectral Unmixing, *IEEE Transactions on Geoscience and Remote Sensing*, vol.52, no.1, pp.341-354, 2014.

[8] C. Deng, S. Zhang, S. Wang, W. Tian and Z. Wu, Sparse hyperspectral unmixing based on smoothed L0 regularization, *Infrared Physics and Technology*, vol.67, pp.306-314, 2014.

[9] E. J. Candès, M. B. Wakin and S. P. Boyd, Enhancing Sparsity by Reweighted l_1 Minimization, *Journal of Fourier Analysis and Applications*, vol.14, no.5, pp.877-905, 2008.

[10] R. Wang, H. C. Li, W. Liao and A. Pizurica, Double reweighted sparse regression for hyperspectral unmixing, *IEEE International Geoscience and Remote Sensing Symposium (IGARSS)*, pp.6986-6989, 2016.

[11] S. Zhang, J. Li, H. Li, C. Deng and A. Plaza, Spectral-Spatial Weighted Sparse Regression for Hyperspectral Image Unmixing, *IEEE Transactions on Geoscience and Remote Sensing*, vol.56, no.6, pp.3265-3276, 2018.

[12] C. Shi and L. Wang, Incorporating spatial information in spectral unmixing: A review, *Remote Sensing of Environment*, vol.149, pp.70-87, 2014.

[13] E. K. Wang, X. Zhang, F. Wang, T. Y. Wu and C. M. Chen, Multilayer Dense Attention Model for Image Caption, *IEEE Access*, vol.7, pp.66358-66368, 2019.

[14] E. Wang, C. M. Chen, M. M. Hassan and A. Almogren, A deep learning based medical image segmentation technique in Internet-of-Medical-Things domain, *Future Generation Computer Systems*, vol.108, pp.135-144, 2020.

[15] K. K. Tseng, R. Zhang, C. M. Chen and M. M. Hassan, DNetUnet: a semi-supervised CNN of medical image segmentation for super-computing AI service, *The Journal of Supercomputing*, vol.77, pp.3594-3615, 2021.

[16] M. D. Iordache, J. Bioucas-Dias and A. Plaza, Total Variation Spatial Regularization for Sparse Hyperspectral Unmixing, *IEEE Transactions on Geoscience and Remote Sensing*, vol.50, no.11, pp.4484-4502, 2012.

[17] R. Wang, H. C. Li, A. Pizurica, J. Li, A. Plaza and W. J. Emery: Hyperspectral Unmixing Using Double Reweighted Sparse Regression and Total Variation, *IEEE Geoscience and Remote Sensing Letters*, vol.14, no.7, pp.1146-1150, 2017.

[18] H. Li, R. Feng, L. Wang, Y. Zhong and L. Zhang, Superpixel-Based Reweighted Low-Rank and Total Variation Sparse Unmixing for Hyperspectral Remote Sensing Imagery, *IEEE Transactions on Geoscience and Remote Sensing*, vol.59, no.1, pp.629-647, 2020.

[19] J. Bioucas-Dias and M. Figueiredo, Alternating direction algorithms for constrained sparse regression: Application to hyperspectral unmixing, *Workshop on Hyperspectral Image and Signal Processing: Evolution in Remote Sensing*, pp.1-4, 2010.
[20] E. Candès and T. Tao, Decoding by linear programming, *IEEE Transactions on Information Theory*, vol.51, no.12, pp.4203-4215, 2005.
[21] E. Candès and T. Tao, Near-Optimal Signal Recovery From Random Projections: Universal Encoding Strategies, *IEEE Transactions on Information Theory*, vol.52, no.12, pp. 5406-5425, 2006.
[22] O. Ozdil and A. Gunes, Unsupervised hyperspectral image segmentation using adaptive bilateral filtering, *Signal Processing and Communications Applications Conference (SIU)*, pp.1010-1013, 2015.
[23] K. Kotwal and S. Chaudhuri, Visualization of Hyperspectral Images Using Bilateral Filtering, *IEEE Transactions on Geoscience and Remote Sensing*, vol.48, no.5, pp.2308-2316, 2010.
[24] H. Peng and R. Rao, Hyperspectral image enhancement with vector bilateral filtering, *IEEE International Conference on Image Processing (ICIP)*, pp.3713-3716, 2009.
[25] C. Tomasi and R. Manduchi, Bilateral filtering for gray and color images, *International Conference on Computer Vision*, pp.839-846, 1998.
[26] X. Li, J. Huang, L. J. Deng and T. Z. Huang, Bilateral filter based total variation regularization for sparse hyperspectral image unmixing, *Information Sciences*, vol.504, pp.334-353, 2019.
[27] R. Achanta, A. Shaji, K. Smith, A. Lucchi, P. Fua and S. Susstrunk, SLIC Superpixels Compared to State-of-the-Art Superpixel Methods, *IEEE Transactions on Pattern Analysis and Machine Intelligence*, vol.34, no.11, pp.2274-2282, 2012.
[28] J. Li, J. M. Bioucas-Dias and A. Plaza, Spectral-Spatial Classification of Hyperspectral Data Using Loopy Belief Propagation and Active Learning, *IEEE Transactions on Geoscience and Remote Sensing*, vol.51, no.2, pp.844-856, 2013.
[29] J. Hou, H. Gao and X. Li, DSets-DBSCAN: A Parameter-Free Clustering Algorithm, *IEEE Transactions on Image Processing*, vol.25, no.7, pp.3182-3193, 2016.
[30] Y. Chen, N. M. Nasrabadi and T. D. Tran, Hyperspectral Image Classification Using Dictionary-Based Sparse Representation, *IEEE Transactions on Geoscience and Remote Sensing*, vol.49, no.10, pp.3973-3985, 2011.
[31] Y. Zhao, J. Yang and J. C. W. Chan, Hyperspectral Imagery Super-Resolution by Spatial-Spectral Joint Nonlocal Similarity, *IEEE Journal of Selected Topics in Applied Earth Observations and Remote Sensing*, vol.7, no.6, pp.2671-2679, 2014.
[32] J. Li, M. Khodadadzadeh, A. Plaza, X. Jia and J. M. Bioucas-Dias, A Discontinuity Preserving Relaxation Scheme for Spectral-Spatial Hyperspectral Image Classification, *IEEE Journal of Selected Topics in Applied Earth Observations and Remote Sensing*, vol.9, no.2, pp.625-639, 2016.
[33] G. Martin and A. Plaza, Region-Based Spatial Preprocessing for Endmember Extraction and Spectral Unmixing, *IEEE Geoscience and Remote Sensing Letters*, vol.8, no.4, pp.745-749, 2011.
[34] G. Martin and A. Plaza, Spatial-Spectral Preprocessing Prior to Endmember Identification and Unmixing of Remotely Sensed Hyperspectral Data, *IEEE Journal of Selected Topics in Applied Earth Observations and Remote Sensing*, vol.5, no.2, pp.380-395, 2012.
[35] R. Clark, G. Swayze, K. Livo, R. Kokaly, S. Sutley, J. Dalton, R. McDougal and C. Gent, Imaging spectroscopy: Earth and planetary remote sensing with the USGS Tetracorder and expert systems, *Journal of Geophysical Research: Planets*, vol.108, no.E12, pp.5131-5135, 2003.